Available online at www.sciencedirect.com

ScienceDirect

Underground Space 6 (2021) 267–280

http://www.keaipublishing.com/en/journals/underground-space/

Predicting jet-grout column diameter to mitigate the environmental impact using an artificial intelligence algorithm

Zhi-Feng Wang [a,b], Wen-Chieh Cheng [c,d,*]

[a] School of Highway, Chang'an University, Xi'an 710064, China
[b] Department of Statistics, Virginia Polytechnic Institute and State University, Blacksburg 24060, United States
[c] School of Civil Engineering, Xi'an University of Architecture and Technology, Xi'an 710055, China
[d] Shaanxi Key Laboratory of Geotechnical and Underground Space Engineering (XAUAT), Xi'an 710055, China

Received 5 February 2020; received in revised form 11 February 2020; accepted 11 February 2020
Available online 25 March 2020

Abstract

This paper describes an approach for predicting the diameter of a jet-grout column using the support vector regression (SVR) technique, which is regarded as a novel learning machine based upon recent advances in statistical theory, in which the combined effects of the construction (construction methods and jetting parameters) and soil properties (soil type and shearing resistance) are considered. Four different kernel functions, namely, a linear kernel function, polynomial kernel function, radial basis kernel function, and sigmoid kernel function, are integrated into the SVR technique. A large amount of field measured data on the diameter of jet-grout column are retrieved from the published literature for training and testing purposes. The results indicate that the SVR technique with a radial basis kernel function provides predictions closest to the measured results, whereas the prepared design charts enable the ability to significantly widen the application of the proposed approach to the areas of ground improvement and environmental protection.

Keywords: Jet grouting; Support vector regression; Machine learning; Radial basis function

1 Introduction

Jet grouting is one of the most popular ground improvement techniques available (Coulter & Martin, 2006; Hossain & Yin, 2013a; Shen, Wang, Sun, Wang, and Horpibulsuk, 2013, Shen, Wang, Horpibulsuk, and Kim, 2013c; Tan & Lu, 2017; Tan, Wei, Zhou, & Diao, 2015; Toraldo, Modoni, Ochmański, & Croce, 2018; Wang, Wang, & Cheng, 2019a; Wang, Shen, & Modoni, 2019b; Wang, Cheng, & Wang, 2018a, Wang, Shen, & Cheng, 2018c; Wei, Gao, Wang, & Zhong, 2019a; Wei, Wu, Yao, Gao, 2019b) and possesses a superior ability to deal with the reinforcement of an embankment foundation (Han, Wang, Al-Naddaf, & Xu, 2017; Jamsawang, Voottipruex, Boathong, Mairaing, & Horpibulsuk, 2015; Jamsawang, Jamnam, Jongpradist, Tanseng, & Horpibulsuk, 2017; Shen, Wang, & Cheng, 2017; Wang, Cheng, & Wang, 2018b), ground improvement during a braced excavation, and the prevention and mitigation of tunneling-induced geohazards (Cheng, Li, Liu, Xu, & Horpibulsuk, 2020; Fu, Yu, Wang, & Yang, 2018; Ho, 2016; Lai, Fan, Chen, Qiu, & Wang, 2015; Lai et al., 2017; Modoni & Bzòwka, 2012; Modoni, Flora, Lirer, Ochmański, & Croce, 2016; Ochmański, Modoni, & Bzòwka, 2015a; Qiu, Xie, Fan, Wang, & Zhang, 2017, Qiu et al., 2018; Zhang, Yang, Zhang, & Gao, 2018). According to the differences in injected fluids used, jet grouting can be categorized into three systems (Ni & Cheng, 2014; Njock, Chen, Modoni, Arulrajah, & Kim, 2018a; Njock, Shen, Modoni, & Arulrajah, 2018b; Wang, Shen, Ho, & Kim, 2013): (1) a single fluid system (injection of a highly pressurized grout), (2) double fluid systems (injection of highly pressurized

* Corresponding author at: School of Highway, Chang'an University, Xi'an 710064, China.
E-mail address: w-c.cheng@xauat.edu.cn (W.-C. Cheng).

https://doi.org/10.1016/j.undsp.2020.02.004

grout and compressed air), and (3) triple fluid systems (injection of highly pressurized water, compressed air, and low pressurized grout). Among these jet grouting systems, the diameter of a jet-grout column installed with a triple fluid system is the largest when the geological conditions and jetting parameters remain the same (Wang, Shen, Ho, & Xu, 2014).

Predicting the diameter of jet-grout columns has been deemed a key issue in the design phase, and several researchers have made contributions toward an appropriate estimation of the jet-grout column diameter. Despite the correlations between the diameter of the jet-grout column and the jetting parameters and soil properties, such relationships are empirically based and do not have a clear physical meaning. Several theoretical methods have also been developed in accordance with the turbulent jet theory and soil mechanics. Modoni, Croce, and Mongiovi (2006) proposed an approach to estimate the diameter of a jet-grout column installed using a single fluid system, in which a seepage model deals with the installation of gravelly soils, whereas an erosion model is used to handle the installation of sandy and clayey soils. Ho (2007) also provided a simplified method for calculating the column diameter by considering the jetting parameters. Shen, Wang, Yang, and Ho (2013b) and Flora, Modoni, Lirer, and Croce (2013) extended the previously mentioned theoretical methods for predicting the diameter of a jet-grout column installed using single, double, and triple fluid systems. With these theoretical methods, the interaction between the highly pressurized fluids and the surrounding geology during the jetting process can be satisfactorily addressed. At present, some new jet grouting technologies (such as Super Jet Technology) have been developed and proven capable of producing a larger column diameter than other grouting technologies. However, the column diameter associated with the new jet grouting technologies may not be appropriately predicted using the currently available theoretical methods. Approaches based on both artificial intelligence and machine learning algorithms, which are becoming more popular in the geology and geotechnical engineering communities, may be used to address any issues raised (Das, Samui, & Sabat, 2012; Güllü, 2017; Samui, Sitharam, & Kurup, 2008; Tinoco, Correia, & Cortez, 2018; Zhang et al., 2019a; Zhang, Wu, Li, Wang, & Samui, 2019b; Zhang, Li, Wu, Li, Liu, & Liu, 2020). They can effectively solve engineering problems without making any arbitrary assumptions adopted in the current methods, enhancing the confidence of the predictions. Ochmański, Modoni, and Bzòwka (2015b) established a new approach for predicting a column diameter using artificial neural networks (ANNs), and the results of a comparison with field measurements verified its applicability. However, ANNs have some inherent shortcomings, such as a slow convergence speed and an ambiguous relationship between the input parameters and output results (Goh & Goh, 2007; Padmini, Ilamparuthi, & Sudheer, 2008). A support vector regression (SVR), a new and efficient artificial intelligent-based technique, has been developed based on statistical learning theory for initially solving the classification problems and subsequently, the regression problems considering the ε-insensitive loss function. Because the SVR technique is implemented based on the structural risk minimization principle, it minimizes not only the errors in the training data, but also a bound of the generalization error of the model applied (Debnath & Dey, 2018).

The objective of this study is to propose an approach for predicting the diameter of a jet-grout column using the artificial intelligence algorithm. A large number of field measured data on the column diameter against different geological conditions (coarse grained soil, coarse grained soil with fines content, and fine grained soil) and construction methods (single, double, and triple fluid systems) have been compiled for training and examining the SVR technique with four different kernel functions. The comparisons with the field data verified the applicability of this proposed approach.

2 Problem description

In jet grouting, high-pressurized fluids (grout or water) are injected into the ground from small-diameter nozzles fixed on a rod, eroding the in situ soil. A cylindrical soil-cement column can be formed by mixing the eroded soil with the injected grout, as shown in Fig. 1. Although a direct measurement of the column diameter during jet grouting cannot be conducted, it has been deemed as a key factor during the design phase. The complexity of a soil-grout interaction has also led to certain difficulties in predicting the column diameter. Because the diameter of a jet-grout column is primarily affected by the construction and soil properties, it can be expressed as a function of the construction and soil properties as follows:

$$D_c = f(\text{construction issues, soil properties}), \tag{1}$$

where D_c is the diameter of the jet-grout column.

The effect of the construction on the diameter of a jet-grout column mainly concerns the construction methods (including single, double, and triple fluid systems) and jetting parameters used (such as the withdrawal rate of the rod, the nozzle diameter, the number of nozzles, the flow rate of the injected fluid, the rotation speed of the rod, and the jetting pressure of the fluid). Numerous researchers have considered the specific energy at the nozzle (E_n) as the key parameter representing the effect of the jetting parameters on the column diameter, which can be quantitatively evaluated through the following equations (Croce & Flora, 2000; Flora et al., 2013; Ochmański et al., 2015b):

$$E_n = \frac{\frac{1}{2}mv_0^2}{L} = \frac{\pi}{8}\frac{M\rho d^2 v_0^3}{v_r} \quad \text{MJ/m}, \tag{2}$$

$$v_0 = \frac{4Q}{M\pi d^2} \quad \text{m/s}, \tag{3}$$

$$E_n = 0.9E_p = 0.9\frac{pQ}{v_r} \quad \text{MJ/m}, \tag{4}$$

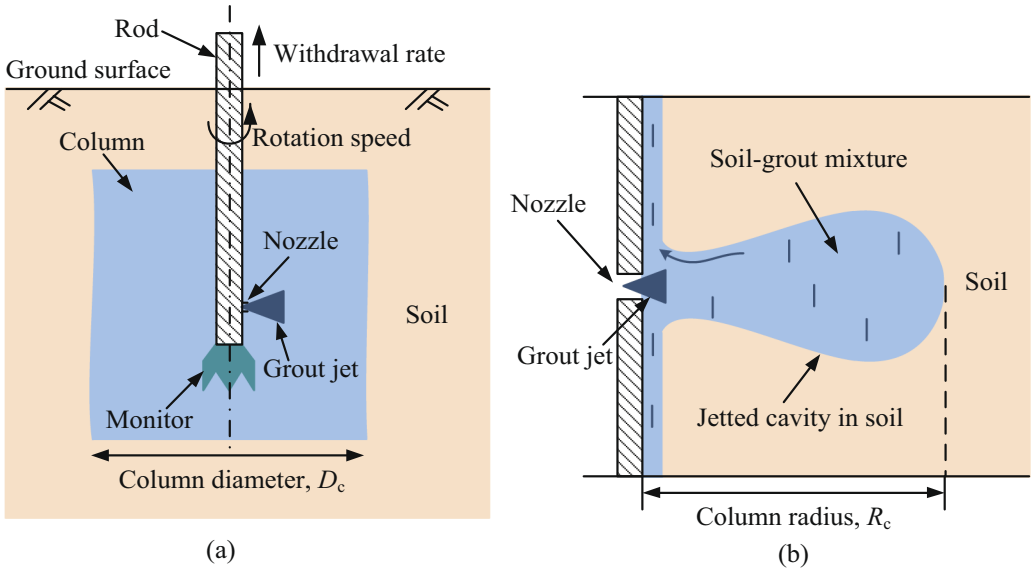

Fig. 1. Schematic illustration of formation of jet-grout column using a single fluid system.

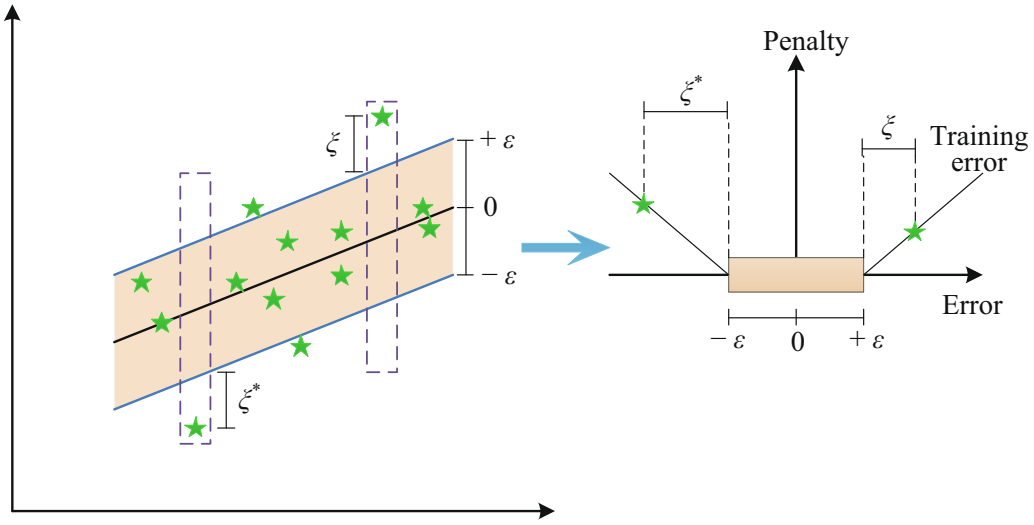

Fig. 2. Description of a linear SVR technique, ε-insensitive loss function, and slack variables.

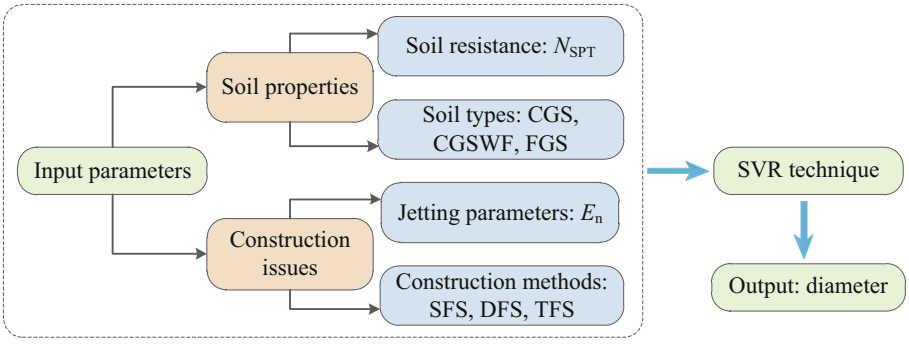

Fig. 3. SVR structure used in this study.

where m is the weight of injected fluid, L is the length of jet-grout column, E_p is the specific energy of the pump, E_n is the specific energy at the nozzle, M is the number of nozzles, ρ is the density of the injected fluids (grout or water), d is the diameter of the nozzles, v_0 is the exit velocity of fluids at the nozzle, Q is the flow rate of the fluid, p is the jetting pressure at the pump, and v_r is the withdrawal rate of the rod.

Table 1
Data collected for training in SVR model (CGS).

Column number	Soil types	Soil resistance	Jetting parameter	Measured diameters	Construction method	References
		N_{spt}	E_n (MJ/m)	D_c (m)		
1	Sandy gravel	10	8.2	0.97	SFS	Bianco and Santoro (1995)
2	Dense sandy gravel	20	13.2	1.10	SFS	Croce, Gaio, Mongiovı‘, and Zaninetti (1994)
3	Dense sandy gravel	20	14.6	1.20	SFS	Croce et al. (1994)
4	Gravelly sand	34	16.8	0.84	SFS	Croce, Modoni, and Carletto (2011)
5	Gravelly sand	28	15.4	0.76	SFS	Croce et al. (2011)
6	Gravelly sand	28	20.3	0.91	SFS	Croce et al. (2011)
7	Gravelly sand	23	22.1	1.08	SFS	Croce et al. (2011)
8	Gravelly sand	34	29.4	1.04	SFS	Croce et al. (2011)
9	Pyroclastic silt and gravely sand	14	16.9	1.11	SFS	Flora et al. (2013)
10	Gravelly sand and gravelly silt	28	15.2	1.00	SFS	Flora et al. (2013)
11	Sand	8	23.8	1.20	SFS	Kimpritis, Standing, and Thurner (2018)
12	Sand	10	38.8	1.30	SFS	Kimpritis et al. (2018)
13	Sand	50	120.1	1.35	SFS	Kimpritis et al. (2018)
14	Sand	9	38.8	1.36	SFS	Kimpritis et al. (2018)
15	Sand	50	130.2	1.46	SFS	Kimpritis et al. (2018)
16	Sand	48	104.0	1.47	SFS	Kimpritis et al. (2018)
17	Sand	46	104.0	1.51	SFS	Kimpritis et al. (2018)
18	Sand	48	111.5	1.52	SFS	Kimpritis et al. (2018)
19	Sand	46	104.0	1.61	SFS	Kimpritis et al. (2018)
20	Sand	50	130.2	1.67	SFS	Kimpritis et al. (2018)
21	Sand	27	77.8	1.70	SFS	Kimpritis et al. (2018)
22	Sand	19	70.7	1.71	SFS	Kimpritis et al. (2018)
23	Sand	10	77.8	1.84	SFS	Kimpritis et al. (2018)
24	Sand	9	77.8	2.00	SFS	Kimpritis et al. (2018)
25	Sand	25	4.5	0.80	DFS	Modoni and Bzòwka (2012)
26	Gravelly sand and sandy gravel	50	17.2	1.00	DFS	Flora et al. (2013)
27	Gravelly sand and sandy gravel	50	18.7	1.00	DFS	Flora et al. (2013)
28	Gravelly sand and sandy gravel	50	21.5	1.00	DFS	Flora et al. (2013)
29	Pyrocalstic silty and gravelly sand	14	16.1	1.50	DFS	Flora et al. (2013)
30	Pyrocalstic silty and gravelly sand	14	21.2	1.70	DFS	Flora et al. (2013)
31	Medium to gravelly sand	24	155.0	2.30	DFS	Ochmański et al. (2015b)
32	Sand	6	134.0	4.50	DFS	Cheng, Ni, Shen, and Huang (2017)
33	Medium to gravelly sand	24	150.0	3.20	TFS	Ochmański et al. (2015b)
34	Medium to gravelly sand	24	270.0	3.50	TFS	Ochmański et al. (2015b)

Table 2
Data collected for training in SVR model (CGSWF).

Column number	Soil types	Soil resistance	Jetting parameter	Measured diameters	Construction method	References
		N_{spt}	E_n (MJ/m)	D_c (m)		
1	Dense silty and gravelly sand	15	9.0	0.66	SFS	Croce and Flora (1998)
2	Dense silty and gravelly sand	15	18.8	0.96	SFS	Croce and Flora (1998)
3	Dense silty and gravelly sand	15	13.4	0.69	SFS	Croce and Flora (1998)
4	Dense silty and gravelly sand	15	18.8	0.97	SFS	Croce and Flora (1998)
5	Dense silty and gravelly sand	15	13.3	0.71	SFS	Croce and Flora (1998)
6	Dense silty and gravelly sand	15	23.5	0.95	SFS	Croce and Flora (1998)
7	Medium loose silty sand	8	7.2	0.69	SFS	Tornaghi and Pettinaroli (2004)
8	Gravel in silty sand matrix	18	7.4	0.60	SFS	Tornaghi and Pettinaroli (2004)
9	Gravel in silty sand matrix	18	14.4	0.70	SFS	Tornaghi and Pettinaroli (2004)
10	Silty sand	10	21.6	0.78	SFS	Tornaghi and Pettinaroli (2004)
11	Pyroclastic silty sand	13	11.5	0.83	SFS	Flora et al. (2013)
12	Medium loose silty sand	8	18.0	1.40	DFS	Tornaghi and Pettinaroli (2004)
13	Medium loose silty sand	8	24.0	1.40	DFS	Tornaghi and Pettinaroli (2004)
14	Medium loose silty sand	8	31.0	1.50	DFS	Tornaghi and Pettinaroli (2004)
15	Silty sand	10	20.7	1.21	DFS	Tornaghi and Pettinaroli (2004)
16	Silty sand	10	19.8	1.19	DFS	Tornaghi and Pettinaroli (2004)
17	Silty sand	10	35.1	1.30	DFS	Tornaghi and Pettinaroli (2004)
18	Silty sand	10	36.9	1.31	DFS	Tornaghi and Pettinaroli (2004)
19	Silty sand	10	13.5	1.28	DFS	Tornaghi and Pettinaroli (2004)
20	Silty sand	10	31.5	1.44	DFS	Tornaghi and Pettinaroli (2004)
21	Silty sand	10	18.9	1.45	DFS	Tornaghi and Pettinaroli (2004)
22	Silty sand	10	34.2	1.63	DFS	Tornaghi and Pettinaroli (2004)
23	Silty sand	10	34.2	1.69	DFS	Tornaghi and Pettinaroli (2004)
24	Silty sand	10	40.5	1.67	DFS	Tornaghi and Pettinaroli (2004)
25	Silty sand	10	73.8	1.93	DFS	Tornaghi and Pettinaroli (2004)
26	Silty sand	10	29.7	1.98	DFS	Tornaghi and Pettinaroli (2004)
27	Silty sand	10	62.1	2.04	DFS	Tornaghi and Pettinaroli (2004)
28	Silty sand	10	30.6	2.17	DFS	Tornaghi and Pettinaroli (2004)
29	Pyroclastic silty sand	13	9.1	0.90	DFS	Flora et al. (2013)
30	Pyroclastic silty sand	13	17.5	1.20	DFS	Flora et al. (2013)
31	Pyroclastic silty sand	13	15.6	1.20	DFS	Flora et al. (2013)
32	Pyroclastic silty sand	13	20.4	1.40	DFS	Flora et al. (2013)
33	Pyroclastic silty sand	13	30.3	1.80	DFS	Flora et al. (2013)
34	Pyroclastic silty sand	13	42.1	1.60	DFS	Flora et al. (2013)
35	Pyroclastic silty sand	13	49.8	1.80	DFS	Flora et al. (2013)
36	Pyroclastic silty sand	13	26.6	1.80	DFS	Flora et al. (2013)
37	Pyroclastic silty sand	13	49.6	1.80	DFS	Flora et al. (2013)
38	Silty sand	3	7.2	0.95	DFS	Durgunoglu et al. (2003)
39	Silty sand	3	8.8	1.10	DFS	Durgunoglu et al. (2003)
40	Silty sand	3	8.5	1.05	DFS	Durgunoglu et al. (2003)
41	Silty sand	3	7.2	1.10	DFS	Durgunoglu et al. (2003)
42	From silty sand to medium sand	12	175.0	2.60	DFS	Stark et al. (2012)
43	Medium loose silty sand	8	85.0	1.90	TFS	Tornaghi and Pettinaroli (2004)
44	Medium loose silty sand	8	42.0	1.65	TFS	Tornaghi and Pettinaroli (2004)
45	Medium loose silty sand	8	25.0	1.63	TFS	Tornaghi and Pettinaroli (2004)
46	Medium loose silty sand	8	31.0	1.50	TFS	Tornaghi and Pettinaroli (2004)

47	Medium loose silty sand	8	22.5	1.50	TFS	Tornaghi and Pettinaroli (2004)	
48	Medium loose silty sand	8	22.5	1.22	TFS	Tornaghi and Pettinaroli (2004)	
49	Medium loose silty sand	8	20.0	1.48	TFS	Tornaghi and Pettinaroli (2004)	
50	Medium loose silty sand	8	13.0	1.45	TFS	Tornaghi and Pettinaroli (2004)	
51	Medium loose silty sand	8	18.0	1.60	TFS	Tornaghi and Pettinaroli (2004)	
52	Medium loose silty sand	8	18.0	1.40	TFS	Tornaghi and Pettinaroli (2004)	
53	Medium loose silty sand	8	15.0	1.30	TFS	Tornaghi and Pettinaroli (2004)	
54	Medium loose silty sand	8	12.0	1.10	TFS	Tornaghi and Pettinaroli (2004)	
55	From silty sand to medium sand	12	220.0	3.00	TFS	Stark et al. (2009)	
56	Silty sand	10	97.0	2.32	TFS	Tornaghi and Pettinaroli (2004)	
57	Silty sand	10	97.0	2.28	TFS	Tornaghi and Pettinaroli (2004)	
58	Silty sand	10	98.0	2.25	TFS	Tornaghi and Pettinaroli (2004)	
59	Silty sand	10	98.0	2.02	TFS	Tornaghi and Pettinaroli (2004)	
60	Silty sand	10	87.0	2.07	TFS	Tornaghi and Pettinaroli (2004)	
61	Sandy silt and silty sand	30	91.0	2.00	TFS	Shen, Wang, Yang, and Ho (2013b)	
62	Sandy silt and silty sand	30	107.0	2.20	TFS	Shen, Wang, Yang, and Ho (2013b)	
63	Sandy silt and silty sand	30	109.0	2.30	TFS	Shen, Wang, Yang, and Ho (2013b)	

Because the soil properties may vary based on the fines content, data on the classification of the soil must be obtained (Cheng, Ni, Shen, & Huang, 2017; Cheng, Ni, Arulrajah, & Huang, 2018; Cheng, Ni, Huang, & Shen, 2019a; Cheng, Wang, & et al,. 2019b; Cheng, Xue, & et al., 2019c; Lu, Wang, Cheng, Yang, & Luo, 2019). In general, soil can be classified into three categories, namely, a coarse grained soil without fines content (CGS), coarse grained soil with fines content (CGSWF), and fine grained soil (FGS), in accordance with the Unified Soil Classification System (ASTM, 2000). The erodibility of soil in response to a high-pressurized fluid jet gradually decreases with an increase in the fines content. However, if the fines content of soils is almost the same, the blow count, N_{SPT}, is utilized as the key parameter to reflect the effect of soil resistance on the column diameter. To sum it up, this problem may be solved using an approach capable of considering the effects of the construction (construction method and jetting parameters) and soil properties (soil type and shearing resistance) on the diameter of a jet-grout column.

3 Development of support vector regression

At present, the computer programs that achieve the best predictive performance are support vector machines (SVMs), which is due to the fact that SVMs are designed to maximize the margin and separate two different classes; thus the trained model generalizes well on unseen data. The principle of the SVR technique is introduced briefly in this section.

Taking a series of training data into account$\{(\boldsymbol{x}_1, y_1),\ldots, (\boldsymbol{x}_n, y_n)\}$, $\boldsymbol{x} \in \boldsymbol{R}^m$, $\boldsymbol{y} \in \boldsymbol{R}$, where $\boldsymbol{x}$ is the input parameter, $\boldsymbol{y}$ is the output parameter, n is the number of collected data, $\boldsymbol{R}^m$ is an m-dimensional vector space, and $\boldsymbol{R}$ is a one-dimensional vector space. Figure 2 shows the principle of a linear SVR technique, ε-insensitive loss function, and slack variables. As can be observed, the shaded area is called an ε-insensitive tube. For the training data outside an ε-insensitive tube, they will be given a nonzero slack variable. When the predicted data are inside the ε-insensitive tube, there will be no differences, which indicates that the value of ε-insensitive loss is zero. When the predicted data are outside the ε-insensitive tube, the value of the loss will be equal to the magnitude of the difference between the estimated data and the tube radius ε (Debnath & Dey, 2018). The ε-insensitive loss function may be determined through the following equation:

$$L_\varepsilon(y) = |y - f(x)|_\varepsilon = \begin{cases} 0, & \text{if } |y - f(x)| \leqslant \varepsilon \\ |y - f(x)| - \varepsilon, & \text{otherwise} \end{cases}, \tag{5}$$

where $L_\varepsilon(y)$ is the loss function.

The linear function for an SVR can generally be obtained through the following equation:

Table 3
Data collected for training in SVR model (FGS).

Column number	Soil types	Soil resistance	Jetting parameter	Measured diameters	Construction method	References
		N_{spt}	E_n (MJ/m)	D_c (m)		
1	Medium stiff clayey sand silt	3	14.4	0.63	SFS	Tornaghi and Pettinaroli (2004)
2	Stiff sandy silt	7	5.9	0.39	SFS	Tornaghi and Pettinaroli (2004)
3	Soft silty clay	3	9.0	0.63	SFS	Tornaghi and Pettinaroli (2004)
4	Very soft clayey silt	2	10.8	0.64	SFS	Tornaghi and Pettinaroli (2004)
5	Clay	10	9.7	0.39	SFS	Croce et al. (2011)
6	Clay	10	7.0	0.38	SFS	Croce et al. (2011)
7	Clay	10	6.7	0.39	SFS	Croce et al. (2011)
8	Clay	10	7.2	0.40	SFS	Croce et al. (2011)
9	Clay	10	9.8	0.42	SFS	Croce et al. (2011)
10	Clay	10	7.4	0.50	SFS	Croce et al. (2011)
11	Clay	10	7.6	0.53	SFS	Croce et al. (2011)
12	Clay	10	7.7	0.47	SFS	Croce et al. (2011)
13	Clay	15	9.4	0.40	SFS	Croce et al. (2011)
14	Clay	15	9.3	0.43	SFS	Croce et al. (2011)
15	Clay	15	15.9	0.49	SFS	Croce et al. (2011)
16	Clay	13	16.4	0.57	SFS	Croce et al. (2011)
17	Clay	13	15.2	0.59	SFS	Croce et al. (2011)
18	Clay	13	20.0	0.64	SFS	Croce et al. (2011)
19	Clay	13	21.6	0.54	SFS	Croce et al. (2011)
20	Clay	13	28.9	0.50	SFS	Croce et al. (2011)
21	Clay	13	16.2	0.45	SFS	Croce et al. (2011)
22	Clay	13	21.6	0.53	SFS	Croce et al. (2011)
23	Clay	13	11.2	0.44	SFS	Croce et al. (2011)
24	Clay	13	12.2	0.40	SFS	Croce et al. (2011)
25	Clay	13	20.3	0.47	SFS	Croce et al. (2011)
26	Clay	13	11.7	0.40	SFS	Croce et al. (2011)
27	Clay	13	9.6	0.43	SFS	Croce et al. (2011)
28	Stiff clay	4	13.4	0.63	SFS	Davie et al. (2003)
29	Sandy silt	10	9.2	0.52	SFS	Bianco and Santoro (1995)
30	Soft clayey silt	5	18.0	0.85	DFS	Tornaghi and Pettinaroli (2004)
31	Soft silty clay	9	22.2	0.61	DFS	Flora et al. (2013)
32	Soft silty clay	9	26.2	1.02	DFS	Flora et al. (2013)
33	Soft silty clay	9	29.8	0.91	DFS	Flora et al. (2013)
34	Soft silty clay	9	29.8	0.70	DFS	Flora et al. (2013)
35	Soft clay	7	31.6	0.80	DFS	Flora et al. (2013)
36	Lean clay or plastic silt	5	36.0	1.09	TFS	Nikbakhtan and Osanloo (2009)
37	Clayey silt and soft clay	3	91.0	2.50	TFS	Shen, Wang, Yang, Ho (2013b)
38	Clayey silt and soft clay	3	107.0	3.00	TFS	Shen, Wang, Yang, and Ho (2013b)
39	Clayey silt and soft clay	3	109.0	3.20	TFS	Shen, Wang, Yang, and Ho (2013b)
40	Stiff silty clay	15	91.0	0.90	TFS	Shen, Wang, Yang, and Ho (2013b)
41	Stiff silty clay	15	107.0	1.00	TFS	Shen, Wang, Yang, and Ho (2013b)
42	Stiff silty clay	15	109.0	1.00	TFS	Shen, Wang, Yang, and Ho (2013b)
43	Clay	23	45.5	1.17	TFS	Kimpritis et al. (2018)
44	Clay	50	137.4	1.34	TFS	Kimpritis et al. (2018)
45	Clay	29	91.3	1.35	TFS	Kimpritis et al. (2018)
46	Clay	20	91.3	1.42	TFS	Kimpritis et al. (2018)
47	Clay	7	68.0	1.46	TFS	Kimpritis et al. (2018)
48	Clay	16	68.0	1.53	TFS	Kimpritis et al. (2018)
49	Clay	22	91.3	1.72	TFS	Kimpritis et al. (2018)

$$f(x) = \langle \boldsymbol{w} \cdot \boldsymbol{x} \rangle + b, \tag{6}$$

where b is the bias, $\boldsymbol{w}$ is the weight vector, and $\langle \boldsymbol{w} \cdot \boldsymbol{x} \rangle$ is the inner product of $\boldsymbol{w}$ and $\boldsymbol{x}$.

With an SVR, the main goal is to find a function $f(x)$ that has the ability to minimize the complexity of the model (Cortes & Vapnik, 1995; Debnath & Dey, 2018). The aforementioned goal can be achieved through a minimization of the weight vector ($\boldsymbol{w}$):

$$\min \frac{1}{2} \| \boldsymbol{w} \|^2$$
$$\text{subjected to } \begin{cases} y_i - \langle \boldsymbol{w} \cdot \boldsymbol{x}_i \rangle - b \leq \varepsilon \\ \langle \boldsymbol{w} \cdot \boldsymbol{x}_i \rangle + b - y_i \leq \varepsilon \end{cases}. \tag{7}$$

However, through the introduction of slack parameters ξ_i and ξ_i^* ($i = 1,\cdots,n$), the estimation error of the training data outside the ε-insensitive tube can be incorporative. The function of a convex optimization can be determined through the following equation:

$$\min \varphi(\boldsymbol{w}, \xi, \xi^*) = \frac{1}{2} \| \boldsymbol{w} \|^2 + C \sum_{i=1}^{n} (\xi_i + \xi_i^*)$$
$$\text{subject to } \begin{cases} y_i - \langle \boldsymbol{w} \cdot \boldsymbol{x}_i \rangle - b \leqslant \varepsilon + \xi_i \\ \langle \boldsymbol{w} \cdot \boldsymbol{x}_i \rangle + b - y_i \leqslant \varepsilon + \xi_i^* \\ \xi_i, \xi_i^* \geqslant 0 \end{cases}, \tag{8}$$

where C is the penalty parameter, that is, >0. In Eq. (8), the left term $\frac{1}{2} \| \boldsymbol{w} \|^2$ indicates the structural risk, whereas the right term $C \sum_{i=1}^{n} (\xi_i + \xi_i^*)$ indicates the empirical risk. The penalty parameter C determines the trade-off between the term $\frac{1}{2} \| \boldsymbol{w} \|^2$ and the empirical risk. By introducing a Lagrange function, the function in Eq. (8) can be transformed as follows:

$$\max L(\alpha^*, \alpha) = -\varepsilon \sum_{i=1}^{n} (\alpha_i^* + \alpha_i) + \sum_{i=1}^{n} y_i (\alpha_i^* - \alpha_i) - \frac{1}{2} \sum_{i=1}^{n} \sum_{j=1}^{n} (\alpha_i^* - \alpha_i)(\alpha_i^* + \alpha_i)(\boldsymbol{x}_i \cdot \boldsymbol{x}_j)$$

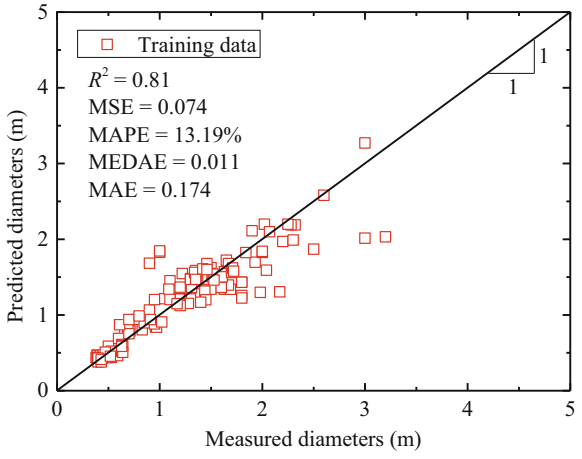

(a) Linear function

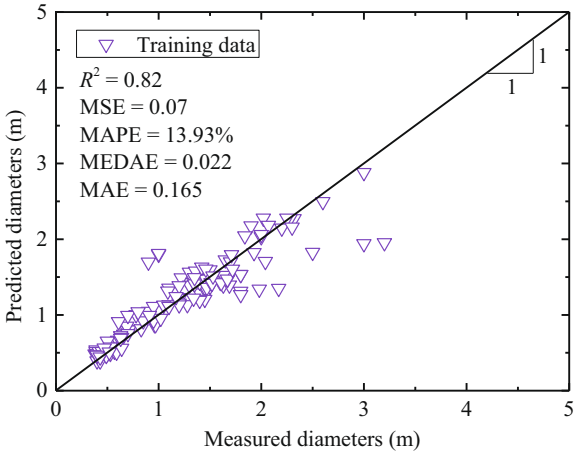

(b) Polynomial function

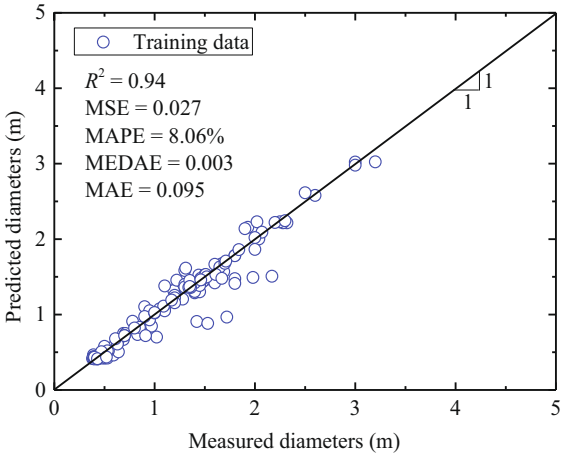

(c) Radial basis function

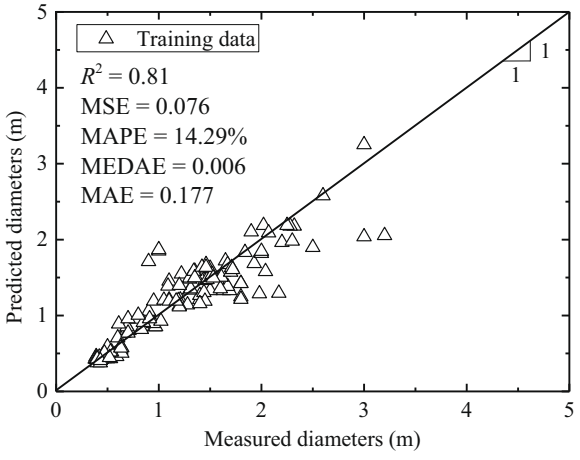

(d) Sigmoid function

Fig. 4. Performance of training data with four different kernel functions: (a) linear, (b) polynomial, (c) radial basis, and (d) sigmoid functions.

$$\text{subject to} \begin{cases} \sum_{i=1}^{n} (\alpha_i^* + \alpha_i) \\ 0 \leqslant \alpha_i^* \leqslant C \\ 0 \leqslant \alpha_i \leqslant C \end{cases}, \tag{9}$$

where α^* and α are Lagrange multipliers, and $L(\alpha^*, \alpha)$ is the Lagrange function. When the Lagrange multipliers after optimization are obtained, the regression problem in Eq. (9) can be expressed as follows:

$$\boldsymbol{w}_0 = \sum_{\text{Support vectors}} (\alpha_i^* + \alpha_i) x_i, \tag{10}$$

$$b_0 = -\frac{1}{2} \boldsymbol{w}_0 [\boldsymbol{x}_r + \boldsymbol{x}_s], \tag{11}$$

$$f(x) = \sum_{\text{Support vectors}} (\alpha_i^* - \alpha_i)(\boldsymbol{x}_i \cdot \boldsymbol{x}) + b_0, \tag{12}$$

where $\boldsymbol{x}_r$ and $\boldsymbol{x}_s$ are the support vectors, b_0 is the optimum value for the bias, and $\boldsymbol{w}_0$ is the optimum value for the weight vector. During the training process of the SVR technique, the values of some Lagrange multipliers can become zero, indicating that these training data can be irrelevant for the final regression analysis. Training modes with non-zero Lagrange multipliers are generally called support vectors (Dibike, Velickov, Solomatine, & Abbott, 2001). The above-mentioned SVR model is capable of solving linear regression problems in general. By introducing a nonlinear kernel function, the following equations can be adopted to solve nonlinear regression problems:

$$f(x) = \sum_{\text{Support vectors}} (\alpha_i^* - \alpha_i) K(\boldsymbol{x}_i \cdot \boldsymbol{x}) + b_0, \tag{13}$$

$$\boldsymbol{w}_0 \cdot \boldsymbol{x} = \sum_{\text{Support vectors}} (\alpha_i^* - \alpha_i) K(\boldsymbol{x}_i, \boldsymbol{x}), \tag{14}$$

$$b_0 = \frac{1}{2} \sum_{\text{Support vectors}} (\alpha_i^* - \alpha_i) [K(\boldsymbol{x}_r, \boldsymbol{x}_i) + K(\boldsymbol{x}_s, \boldsymbol{x}_i)], \tag{15}$$

where $K(\boldsymbol{x}_i \cdot \boldsymbol{x})$ is the kernel function,

$$K(\boldsymbol{x}_i \cdot \boldsymbol{x}) = \langle \phi(x_i) \cdot \phi(x) \rangle. \tag{16}$$

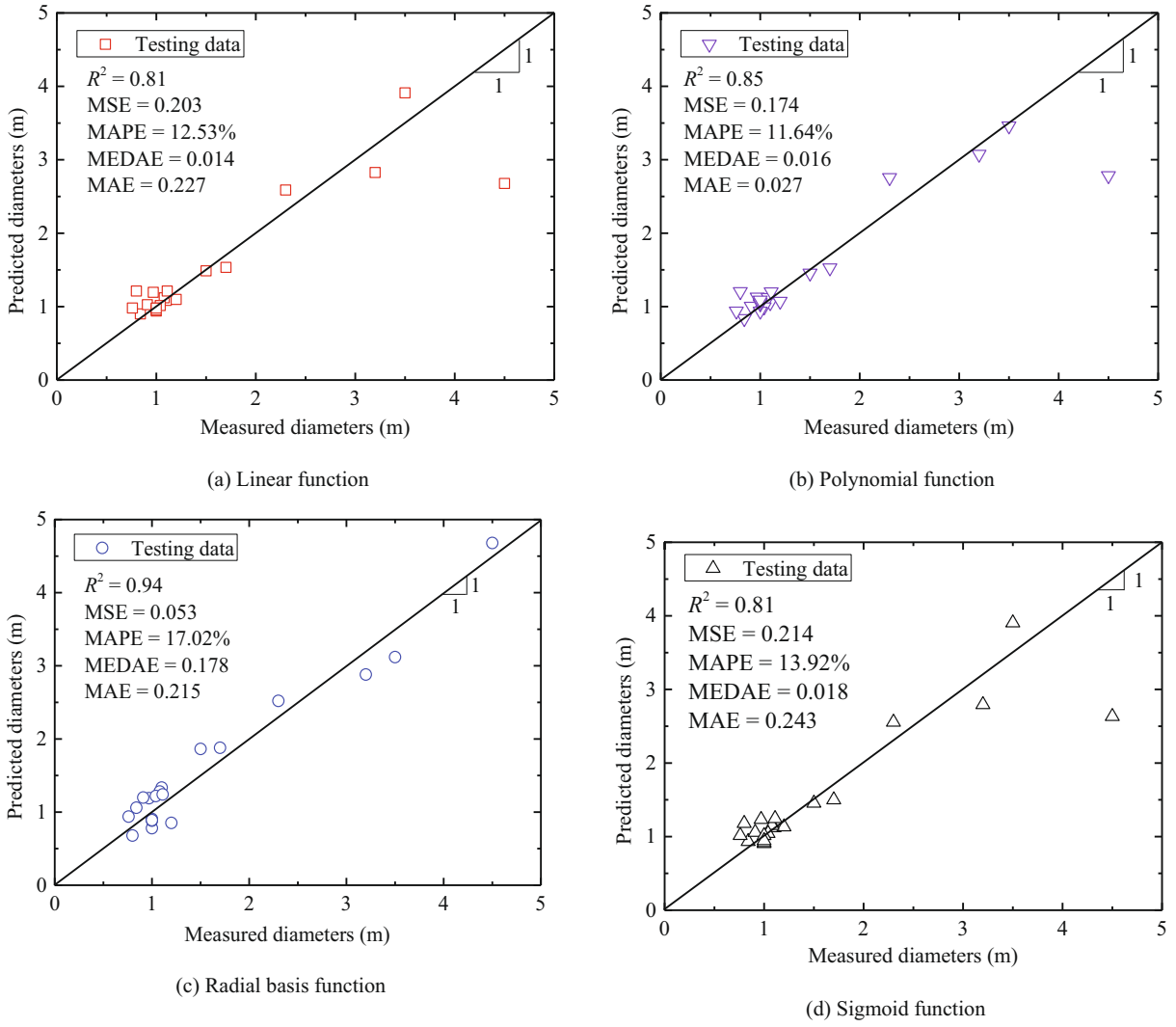

Fig. 5. Performance of testing data with four different kernel functions: (a) linear, (b) polynomial, (c) radial basis, and (d) sigmoid functions.

Through the use of a map ϕ, the input variables can be mapped onto the feature space. The dot product of $\phi(x_i) \cdot \phi(x)$ is calculated using a linear combination of the training data (Samui, 2008).

A structure based on the SVR technique used to predict the diameter of a jet-grout column is established by considering the effects of the construction (construction methods, SFS, DFS, and TFS; jetting parameter, E_n) and soil properties (soil types, CGS, CGSWF, and FGS; soil resistance, N_{SPT}), as shown in Fig. 3. Four different kernel functions, namely, a linear kernel function, polynomial kernel function, radial basis kernel function, and sigmoid kernel function, integrated into the SVR technique are involved in the training process. A total of 146 experimental datasets from several published studies were collected as the training and testing data. Tables 1–3 tabulate the collected diameters of a jet-grout column installed in CGS, CGSWF, and FGS, respectively, using different construction methods (SFS, DFS, and TFS).

4 Analysis of accuracy of predicted results using SVR technique

Five regression indices, namely, a correlation coefficient (R^2), mean squared error (MSE), mean absolute error (MAE), mean absolute percentage error (MAPE), and median absolute error (MEDAE), were incorporated into a series of benchmark tests for assessing the predictive performance of the SVR technique with different kernel functions. The five regression indices can be determined as follows:

$$\text{correlation coefficient}, R = \frac{\sum_{i=1}^{n}\left(l_i - \bar{l_i}\right)\left(m_i - \bar{m_i}\right)}{\sqrt{\sum_{i=1}^{n}\left(l_i - \bar{l_i}\right)^2 \sum_{i=1}^{n}\left(m_i - \bar{m_i}\right)^2}},$$

$$\text{MSE} = \frac{\sum_{i=1}^{n}(l_i - m_i)^2}{n},$$

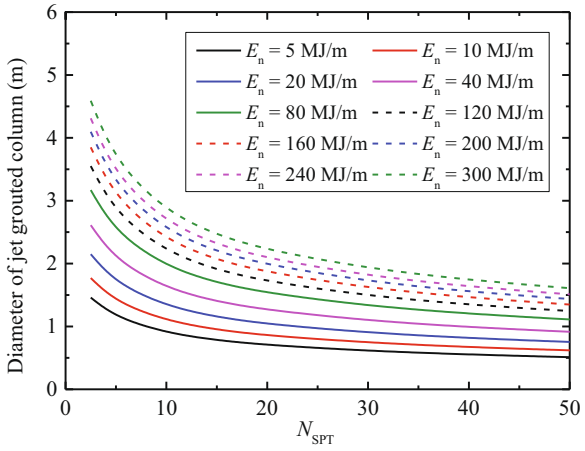

(a) SFS in coarse grained soil without fines content

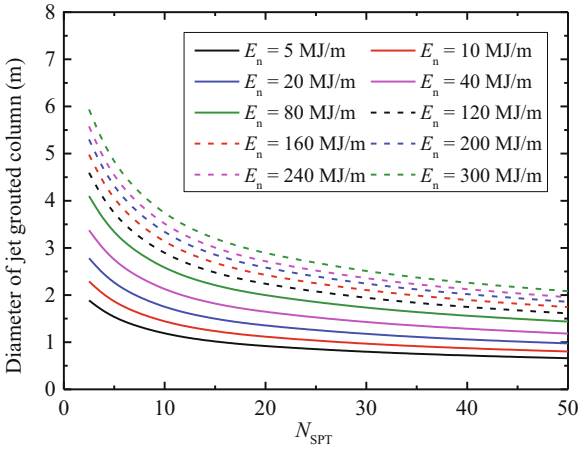

(b) DFS in coarse grained soil without fines content

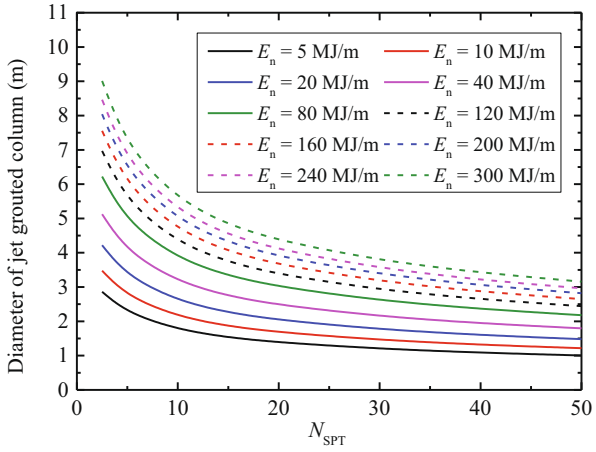

(c) TFS in coarse grained soil without fines content

Fig. 6. Design charts for diameter prediction of jet-grout column in coarse grained soil without fines content using different construction methods: (a) SFS, (b) DFS, and (c) TFS.

$$\mathrm{MAPE} = \frac{100\%}{n} \times \left[\sum_{i=1}^{n}\left|\frac{l_i - m_i}{l_i}\right|\right],$$

$$\mathrm{MEDAE} = \mathrm{median}(l_i - m_i),$$

$$\mathrm{MAE} = \frac{1}{n}\sum_{i=1}^{n}|l_i - m_i|,$$

where l_i is the observed data, m_i is the predicted data, n is the number of adopted data, $\bar{l}_i$ is the average value of the observed data, and $\bar{m}_i$ is the average value of the predicted data.

Figures 4 and 5 show comparisons of the predicted results (training and testing data) resulting from the SVR technique with the four different kernel functions (linear, polynomial, radial basis, and sigmoid functions) used to measure the column diameters. As can be observed, the predicted results from the SVR technique with the radial basis function are the closest to the measured column diameters. The associated regression indices are as follows: $R^2 = 0.94$, MSE = 0.053, MAPE = 17.02%, MEDAE = 0.178, and MAE = 0.215, whereas the SVR technique using the sigmoid kernel function provides the poorest predictions with regression indices of $R^2 = 0.81$, MSE = 0.214, MAPE = 13.92%, MEDAE = 0.018, and MAE = 0.243. It can be suggested from the above results that the SVR technique with the radial basis function has significant potential in the prediction of the jet-grout column diameter. Although the sigmoid kernel function may not be suitable for this case, it is case-dependent and can still be extended to other cases. The proposed method using the SVR technique has a high computing efficiency and the computational effort is low. The calculation time of the proposed method with four different kernel functions is less than 12 s.

5 Design charts for predicting the diameter of jet grouted columns

The SVR technique with a radial basis kernel function has proved to be effective in predicting the diameter of a jet-grout column. However, the complexity of the SVR technique significantly limits its application in general practice. For the sake of convenience, design charts for predicting the diameter of a jet-grout column in different soils against three different construction methods were prepared,

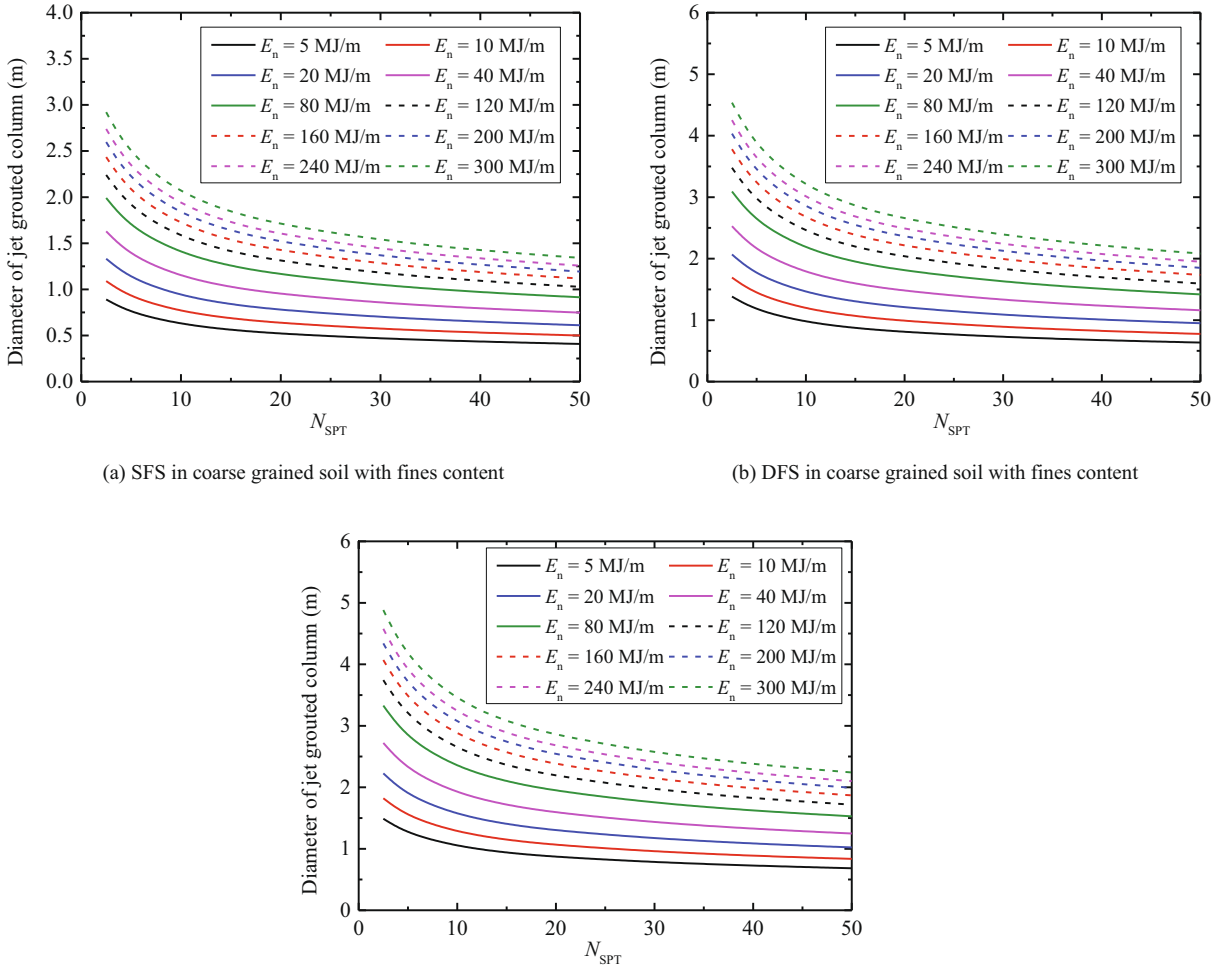

(a) SFS in coarse grained soil with fines content

(b) DFS in coarse grained soil with fines content

(c) TFS in coarse grained soil with fines content

Fig. 7. Design charts for diameter prediction of jet-grout column in coarse grained soil with fines content using different construction methods: (a) SFS, (b) DFS, and (c) TFS.

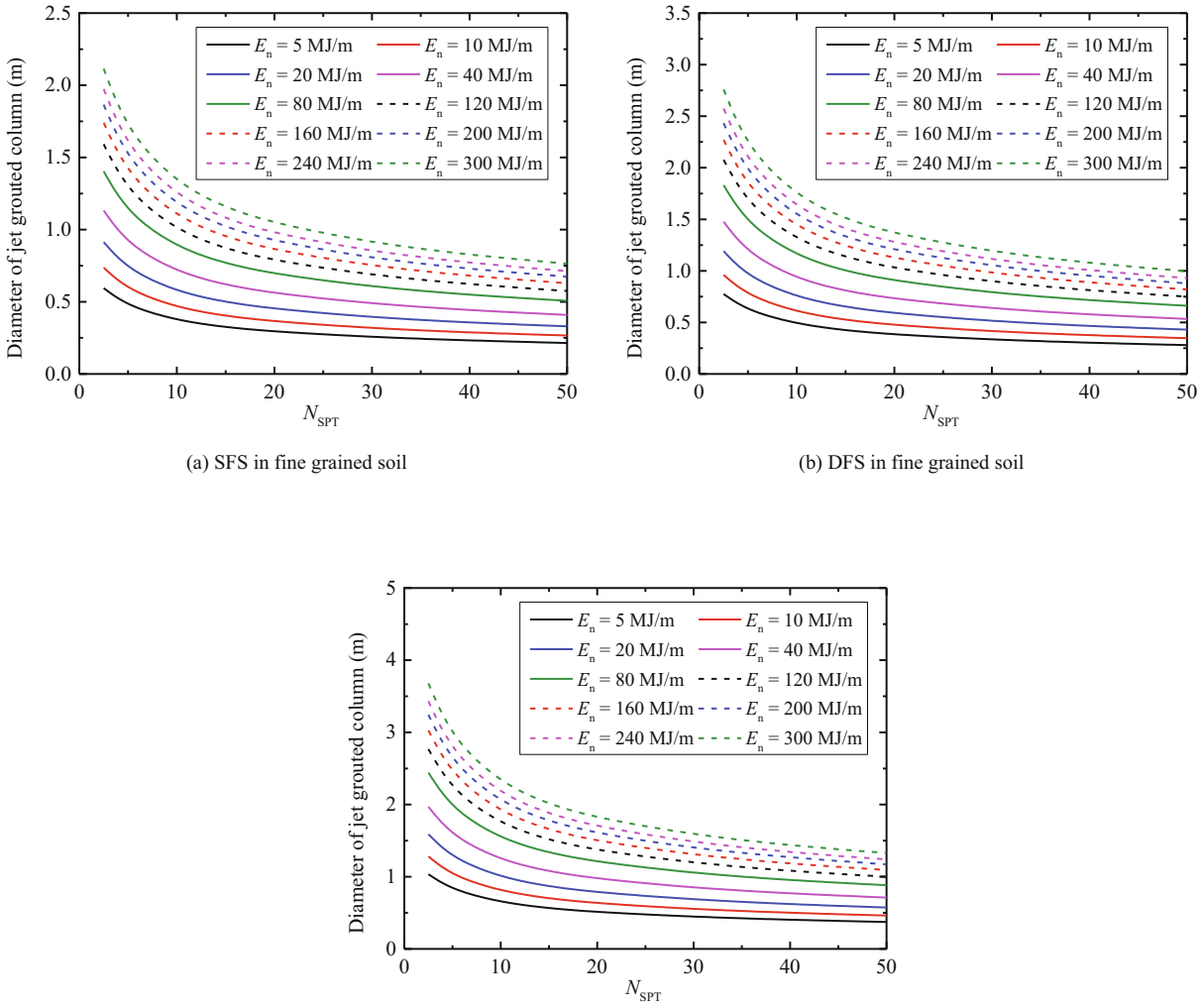

(a) SFS in fine grained soil

(b) DFS in fine grained soil

(c) TFS in fine grained soil

Fig. 8. Design charts for diameter prediction of jet-grout column in fine grained soil using different construction methods: (a) SFS, (b) DFS, and (c) TFS.

as shown in Figs. 6–8. The design charts allow dealing with the effects of the construction and soil properties when predicting the diameter of a jet-grout column during the design phase. The specific energy at the nozzle (E_n) within the range of 5–300 MJ/m, and N_{SPT} values varying from 2.5 to 50, incorporated into the design charts are deemed sufficient and representative of most situations that can be found in engineering practice, thereby widening the application of the SVR technique in the grouting industry.

6 Conclusions

An approach for predicting the diameter of a jet-grout column installed in different soft soils using an artificial intelligent algorithm (an SVR technique) was proposed in this study. Four different kernel functions, namely, a linear, polynomial, radial basis, and sigmoid kernel functions were integrated into the SVR technique. The proposed approach also takes the effects of the construction (construction methods and jetting parameters) and soil properties (soil type and shearing resistance) into account. A total of 146 field measured data on the diameter of a jet-grout column from the published literature were retrieved for training and testing purposes, and it was suggested that the SVR technique with a radial basis kernel function produces the most accurate prediction, allowing practitioners and/or engineers to mitigate any environmental impact from their constructions. The application of the SVR technique by the ground improvement industry can be widened using the proposed design charts.

Data availability

The data used to support the findings of this study are included within the article.

Declaration of Competing Interest

The authors declare that they have no known competing financial interests or personal relationships that could have appeared to influence the work reported in this paper.

Acknowledgements

The research described in this study would not have been possible without financial supports from The Project Supported by Natural Science Basic Research Plan in Shaanxi Province of China (Grant no. 2019JQ-114), the National Nature Science Foundation of China (NSFC) (Grant nos. 41702287 and 41807245) and the Fundamental Research Funds for the Central Universities (Grant no. 300102218517). These financial supports are gratefully acknowledged.

References

ASTM (2000). *Standard practice for classification of soils for engineering purposes (unified soil classification system). D2487*. West Conshohocken, Pa: ASTM International.

Bianco, B., & Santoro, V. M. (1995). L'importanza dei campi sperimentale e delle sperimentazioni nella progettazione dei trattamenti colonnari: L'esempio delle fondazioni del viadotto Rio Matzeu della nuova SS. 131 variante nei pressi di Cagliari. In *Proceeding of the 19th natational conference on geotechnical engineeering* (pp. 81–88) (in Italian).

Cheng, W.-C., Ni, J. C., Shen, J. S.-L., & Huang, H.-W. (2017). Investigation into factors affecting jacking force: A case study. In *Proceedings of the Institution of Civil Engineers - Geotechnical Engineering, 170*(4), 322–334.

Cheng, W. C., Ni, J. C., Arulrajah, A., & Huang, H. W. (2018). A simple approach for characterising tunnel bore conditions based upon pipe-jacking data. *Tunnelling and Underground Space Technology, 71*, 494–504.

Cheng, W. C., Ni, J. C., Huang, H. W., & Shen, J. S. (2019a). The use of tunnelling parameters and spoil characteristics to assess soil types: A case study from alluvial deposits at a pipejacking project site. *Bulletin of Engineering Geology and the Environment, 78*(4), 2933–2942.

Cheng, W. C., Wang, L., Xue, Z. F., Ni, J. C., Rahman, M., & Arulrajah, A. (2019b). Lubrication performance of pipejacking in alluvial deposits. *Tunnelling and Underground Space Technology, 91*, 102991.

Cheng, W. C., Xue, Z. F., Wang, L., & Xu, J. (2019c). Using post-harvest waste to improve shearing behaviour of loess and its validation by multiscale direct shear tests. *Applied Sciences, 9*(23), 5206.

Cheng, W. C., Li, G., Liu, N., Xu, J., & Horpibulsuk, S. (2020). Recent massive incidents for subway construction in soft alluvial deposits of Taiwan: A review. *Tunnelling and Underground Space Technology, 96*, 103178.

Coulter, S., & Martin, C. D. (2006). Effect of jet-grouting on surface settlements above the Aeschertunnel, Switzerland. *Tunnelling and Underground Space Technology, 21*(5), 542–553.

Cortes, C., & Vapnik, V. (1995). Support-vector networks. *Machine Learning, 20*(3), 273–297.

Croce, P., & Flora, A. (2000). Analysis of single-fluid jet grouting. *Géotechnique, 50*(6), 739–748.

Croce, P., & Flora, A. (1998). Jet-grouting effects on pyroclastic soils. *Rivista Italiana di Geotecnica, 32*(2), 5–14.

Croce, P., Modoni, G., & Carletto, M. F. W. (2011). Correlazioni per la previsione del diametro delle colonne di jet grouting. In *Proceedings of the XXIV National Geotechnical Conference, 'Innovazione Tecnologicanell'Ingeg-neria Geotecnica', Associazione Geotecnica Italiana, 22–24 June2011, Napoli* (pp. 423–430) (in Italian).

Croce, P., Gaio, A., Mongiovı̀, L., & Zaninetti, A. (1994). Unaverifica sperimentale degli effetti della gettiniezione. *Rivista Italiana di Geotecnica, 28*(2), 91–101 (in Italian).

Das, S. K., Samui, P., & Sabat, A. K. (2012). Prediction of field hydraulic conductivity of clay liners using an artificial neural network and support vector machine. *International Journal of Geomechanics, 12*(5), 606–611.

Davie, J. R., Piyal, M., Sanver, A., & Tekinturhan, B. (2003). In *Jet Grout Columns Support Major Power Plant Structures*, In *Proceedings of the 12th Pan-American Conference on Soil Mechanics and Geotechnical Engineering*. Cambridge: ASCE Geo-Inatitute.

Dibike, Y., Velickov, S., Solomatine, D., & Abbott, M. (2001). Model induction with support vector machines: Introduction and applications. *Journal of Computing in Civil Engineering, 15*(3), 208–216.

Debnath, P., & Dey, A. K. (2018). Prediction of bearing capacity of geogrid-reinforced stone columns using support vector regression. *International Journal of Geomechanics, 18*(2), 04017147.

Durgunoglu, H. T., Kulac, H. F., Oruc, K., Yildiz, R., Sickling, J., Boys, I. E., ... Emrem, C. (2003). *A case history of ground treatment with jet grouting against liquefaction for a cigarette factory in Turkey. Grouting and ground treatment, Geotechnical special publication 120*. Reston, VA: ASCE (pp. 452–463). Reston, VA: ASCE.

Flora, A., Modoni, G., Lirer, S., & Croce, P. (2013). The diameter of single, double and triple fluid jet grouting columns: Prediction method and field trial results. *Géotechnique, 63*(11), 934–945.

Fu, J. Y., Yu, Z. W., Wang, S. Y., & Yang, J. S. (2018). Numerical analysis of framed building response to tunnelling induced ground movements. *Engineering Structures, 158*, 43–66.

Goh, A. T., & Goh, S. (2007). Support vector machines: Their use in geotechnical engineering as illustrated using seismic liquefaction data. *Computers and Geotechnics, 34*(5), 410–421.

Güllü, H. (2017). A new prediction method for the rheological behavior of grout with bottom ash for jet grouting columns. *Soils and Foundation, 57*(3), 384–396.

Han, J., Wang, F., Al-Naddaf, M., & Xu, C. (2017). Progressive development of two-dimensional soil arching with displacement. *International Journal of Geomechanics, 17*(12), 04017112.

Ho, C. E. (2007). Fluid-soil interaction model for jet grouting. In *Grouting for ground improvement: Innovative concepts and applications. Geotechnical special publication no. 168* (pp. 1–10). Reston: American Society of Civil Engineers (ASCE) Press.

Ho, C. E. (2016). Groundwater management for sustainable underground subway development in Manhattan, New York City. In *Geo-Chicago 2016: Sustainability and resiliency in geotechnical engineering. Geotechnical special publication no. 269* (pp. 663–672). Reston: American Society of Civil Engineers (ASCE) Press.

Hossain, M. A., & Yin, J. H. (2013). Behavior of a pressure-grouted soil-cement interface in direct shear tests. *International Journal of Geomechanics, 14*(1), 101–109.

Jamsawang, P., Jamnam, S., Jongpradist, P., Tanseng, P., & Horpibulsuk, S. (2017). Numerical analysis of lateral movements and strut forces in deep cement mixing walls with top-down construction in soft clay. *Computers and Geotechnics, 88*, 174–181.

Jamsawang, P., Voottipruex, P., Boathong, P., Mairaing, W., & Horpibulsuk, S. (2015). Three-dimensional numerical investigation on lateral movement and factor of safety of slopes stabilized with deep cement mixing column rows. *Engineering Geology, 188*, 159–167.

Kimpritis, T., Standing, J. R., & Thurner, R. (2018). Estimating column diameters in jet-grouting processes. In *Proceedings of the Institution of Civil Engineers - Ground Improvement, 171*(3), 148–158.

Lai, J. X., Fan, H. B., Chen, J. X., Qiu, J. L., & Wang, K. (2015). Blasting vibration monitoring of undercrossing railway tunnel using wireless sensor network. *International Journal of Distributed Sensor Networks, 11*(6), 703980.

Lai, J. X., He, S. Y., Qiu, J. L., Chen, J. X., Wang, L. X., Wang, K., & Wang, J. B. (2017). Characteristics of seismic disasters and aseismic measures of tunnels in Wenchuan earthquake. *Environmental Earth Science, 76*(2), 94.

Lu, J., Wang, T. H., Cheng, W. C., Yang, T., & Luo, Y. (2019). Permeability anisotropy of loess under influence of dry density and freeze-thaw cycles. *International Journal of Geomechanics, 19*(9), 04019103.

Modoni, G., Croce, P., & Mongiovi, L. (2006). Theoretical modelling of jet grouting. *Géotechnique, 56*(5), 335–347.

Modoni, G., & Bzòwka, J. (2012). Analysis of foundation reinforced with jet grouting. *Journal of Geotechnical and Geoenvironmental Engineering, 138*(12), 1442–1454.

Modoni, G., Flora, A., Lirer, S., Ochmański, M., & Croce, P. (2016). Design of jet grouted excavation bottom plugs. *Journal of Geotechnical and Geoenvironmental Engineering, 142*(7), 04016018.

Ni, J. C., & Cheng, W. C. (2014). Quality control of double fluid jet grouting below groundwater table: Case history. *Soils and Foundations, 54*(6), 1039–1053.

Nikbakhtan, B., & Osanloo, M. (2009). Effect of grout pressure and grout flow on soil physical and mechanical properties in jet grouting

operations. *International Journal of Rock Mechanics and Mining Science, 46*(3), 498–505.
Njock, P. G. A., Chen, J., Modoni, G., Arulrajah, A., & Kim, Y. H. (2018a). A review of jet grouting practice and development. *Arabian Journal of Geosciences, 11*(16), 459.
Njock, P. G. A., Shen, J. S., Modoni, G., & Arulrajah, A. (2018b). Recent advances in horizontal jet grouting (HJG): An overview. *Arabian Journal for Science and Engineering, 43*(4), 1543–1560.
Padmini, D., Ilamparuthi, K., & Sudheer, K. P. (2008). Ultimate bearing capacity prediction of shallow foundations on cohesionless soils using neurofuzzy models. *Computers and Geotechnics, 35*(1), 33–46.
Ochmański, M., Modoni, G., & Bzòwka, J. (2015a). Numerical analysis of tunnelling with jet-grouted canopy. *Soils and Foundations, 55*(5), 929–942.
Ochmański, M., Modoni, G., & Bzòwka, J. (2015b). Prediction of the diameter of Jet Grouting columns with Artificial Neural Networks. *Soils and Foundations, 55*(2), 425–436.
Qiu, J. L., Liu, H. Q., Lai, J. X., Lai, H. P., Chen, J. X., & Wang, K. (2018). Investigating the long-term settlement of a tunnel built over improved loessial foundation soil using jet grouting technique. *Journal of Performance Constructed Facilities, 32*(5), 04018066.
Qiu, J., Xie, Y., Fan, H., Wang, Z., & Zhang, Y. (2017). Centrifuge modelling of twin-tunnelling induced ground movements in loess strata. *Arabian Journal of Geosciences, 10*(22), 493.
Samui, P. (2008). Support vector machine applied to settlement of shallow foundations on cohesionless soils. *Computers and Geotechnics, 35*(3), 419–427.
Samui, P., Sitharam, T. G., & Kurup, P. U. (2008). OCR prediction using support vector machine based on piezocone data. *Journal of Geotechnical and Geoenvironmental Engineering, 134*(6), 894–898.
Shen, S. L., Wang, Z. F., & Cheng, W. C. (2017). Estimation of lateral displacement induced by jet grouting in clayey soils. *Géotechnique, 67*(7), 621–630.
Shen, S. L., Wang, Z. F., Sun, W. J., Wang, L. B., & Horpibulsuk, S. (2013a). A field trial of horizontal jet grouting with composite-pipe method in soft deposit of Shanghai. *Tunnelling and Underground Space Technology, 35*, 142–151.
Shen, S. L., Wang, Z. F., Yang, J., & Ho, C. E. (2013b). Generalized approach for prediction of jet grout column diameter. *Journal of Geotechnical and Geoenvironmental Engineering, 139*(12), 2060–2069.
Shen, S. L., Wang, Z. F., Horpibulsuk, S., & Kim, Y. H. (2013c). Jet-Grouting with a newly developed technology: The Twin-Jet method. *Engineering Geology, 152*(1), 87–95.
Stark, T. D., Axtell, P. J., Lewis, R. J., Dillon, J. C., Empson, W. B., Topi, J. E., & Walberg, F. C. (2009). Soil inclusions in jet grout columns. *Deep Foundation Institute Journal, 3*(1), 44–55.
Stark, T. D., Axtell, P. J., Walberg, F. C., Dillon, J. C., Bellew, G. M., & Matthews, D. L. (2012). Jet grouting and safety of Tuttle Creek Dam. *Deep Foundation Institute Journal, 6*(1), 3–20.
Tinoco, J., Correia, A. G., & Cortez, P. (2018). Jet grouting column diameter prediction based on a data-driven approach. *European Journal of Environmental and Civil Engineering, 22*(3), 338–358.
Tan, Y., & Lu, Y. (2017). Forensic diagnosis of a leaking accident during excavation. *Journal of Performance of Constructed Facilities, 31*(5), 04017061.
Tan, Y., Wei, B., Zhou, X., & Diao, Y. (2015). Lessons learned from construction of shanghai metro stations: Importance of quick excavation, prompt propping, timely casting and segmented construction. *Journal of Performance of Constructed Facilities, 29*(4), 04014096.
Toraldo, C., Modoni, G., Ochmański, M., & Croce, P. (2018). The characteristic strength of jet-grouted material. *Géotechnique, 68*(3), 262–279.
Tornaghi, R., & Pettinaroli, A. (2004). Design and control criteria of jet grouting treatments. In *Proceedings of ASEP–GI international symposium sur l'ame´lioration des sols en place* (pp. 1–24). Paris, France: Ecole Nationale des Ponts et Chausse´es.
Wang, Y. Q., Wang, Z. F., & Cheng, W. C. (2019a). A review on land subsidence caused by groundwater withdrawal in Xi'an, China. *Bulletin of Engineering Geology and the Environment, 78*(4), 2851–2863.
Wang, Z. F., Shen, S. L., Ho, C. E., & Kim, Y. H. (2013). Investigation of field installation effects of horizontal Twin-Jet grouting in Shanghai soft soil deposits. *Canadian Geotechnical Journal, 50*(3), 288–297.
Wang, Z.-F., Shen, S.-L., Ho, C.-E., & Xu, Y.-S. (2014). Jet grouting for mitigation of installation disturbance. In *Proceedings of the Institution of Civil Engineers - Geotechnical Engineering, 167*(6), 526–536.
Wang, Z. F., Cheng, W. C., & Wang, Y. Q. (2018a). Investigation into geohazards during urbanization process of Xi'an, China. *Natural Hazards, 92*(3), 1937–1953.
Wang, Z. F., Cheng, W. C., & Wang, Y. Q. (2018b). Simple method to predict settlement of composite foundation under embankment. *International Journal of Geomechanics, 18*(12), 04018158.
Wang, Z. F., Shen, J. S., & Cheng, W. C. (2018c). Simple method to predict ground displacements caused by installing horizontal jet-grouting columns. *Mathematical Problems in Engineering*, 1897394.
Wang, Z. F., Shen, S. L., & Modoni, G. (2019b). Enhancing discharge of spoil to mitigate disturbance induced by horizontal jet grouting in clayey soil: Theoretical model and application. *Computers and Geotechnics, 111*, 222–228.
Wei, Y., Gao, X., Wang, F., & Zhong, Y. (2019a). Nonlinear strain distribution in a field-instrumented concrete pavement slab in response to environmental effects. *Road Materials and Pavement Design, 20*(2), 367–380.
Wei, Y., Wu, Z., Yao, X., & Gao, X. (2019b). Quantifying effect of later curing on pores of paste subject to early age freeze thaw cycles by different techniques. *Journal of Materials in Civil Engineering, 31*(8), 04019153.
Zhang, X. M., Yang, J. S., Zhang, Y. X., & Gao, Y. F. (2018). Cause investigation of damages in existing building adjacent to foundation pit in construction. *Engineering Failure Analysis, 83*, 117–124.
Zhang, W. G., Zhang, R., Wu, C., Goh, A. T. C., Lacasse, S., Liu, Z., & Liu, H. (2019a). State-of-the-art review of soft computing applications in underground excavations. *Geoscience Frontiers*. https://doi.org/10.1016/j.gsf.2019.12.003.
Zhang, W. G., Wu, C., Li, Y., Wang, L., & Samui, P. (2019b). Assessment of pile drivability using random forest regression and multivariate adaptive regression splines. *Georisk: Assessment and Management of Risk for Engineered Systems and Geohazards*. https://doi.org/10.1080/17499518.2019.1674340.
Zhang, W. G., Li, H. R., Wu, C. Z., Li, Y. Q., Liu, Z. Q., & Liu, H. L. (2020). Soft computing approach for prediction of surface settlement induced by earth pressure balance shield tunneling. *Underground Space*. https://doi.org/10.1016/j.undsp.2019.12.003.